CME LIVE OPEN ACCESS

Journal of
Theoretical Physics & Mathematics Research

Research Article ISSN: 3065-8802

On Geometric Origin of Dark Matter, Dark Energy, and the Fine-Structure Constant

Vladimir Trifonov* and Philip V. Trifonov

PT Computing, LLC, P.O. Box 7621, Cumberland RI, USA.

Corresponding Vladimir Trifonov, PT Computing, LLC, P.O. Box 7621, Cumberland RI, USA.

Received: 2026 July 09 **Accepted:** 2026 July 29 **Published:** 2026 Aug 10

Abstract

The ΛCDM model successfully accounts for cosmic expansion and large-scale structure but treats dark matter, dark energy, and the fine-structure constant α as independent inputs. We present an outline of a geometric construction in which all three emerge from the interplay of two natural measures — a metric (Lebesgue-type) measure and an invariant (Haar-type) structural measure — on spacetime. A single crossover scale $r^* = e^{-1}$ and a unified visibility kernel $K(x) = \Sigma(x)\bullet\Pi_{time}$ (with $\Pi_{time} = 1/2$ from the arrow-of-time projection) simultaneously produce the dark-matter-to-baryon ratio $\Omega_{DM}/\Omega_b \approx 6$, suppressed late-time growth of structure, and the leading term of the fine-structure constant $\alpha^{-1} = 4\pi^3 + \pi^2 + \pi \approx 137.03630378$. If successful, the framework would require no new particles, no free parameters, and even at this preliminary stage it can make concrete, falsifiable predictions for current and upcoming cosmological surveys and precision measurements of the fine-structure constant α.

Keywords: ΛCDM Cosmology, Dark Matter, Dark Energy, Fine-structure Constant, Geometric Cosmology, Haar Measure, Lebesgue Measure, Visibility Kernel, Arrow of Time, Structure Formation

1. Introduction

The ΛCDM model reproduces the cosmic microwave background, baryon acoustic oscillations, supernova distances, and large-scale structure with high precision [3,38,47]. Yet the physical nature of its two dominant components — cold dark matter ($\Omega_{DM} \approx 0.27$) and the cosmological constant ($\Omega_\Lambda \approx 0.68$) — remains unknown. Extensive direct-detection experiments have yielded no non-gravitational evidence for dark-matter particles. The observed abundance ratio $\Omega_{DM}/\Omega_b \approx 5.4$ and the value of the fine-structure constant $\alpha \approx 1/137.036$ are likewise introduced by hand. These three puzzles appear unrelated in the standard paradigm. We propose that they share a common geometric origin: the interplay of two natural measures on spacetime and its underlying configuration space. The two measures are automatically produced in a specific geometric modification of quantum mechanics, and the aim of this work is to initiate steps toward the unification within the framework of that particular version of QM.

2. HHQM Kinematics

Hyperhamiltonian quantum mechanics (HHQM) [42,43,44,45], a geometric modification of the standard Quaternionic Quantum Mechanics [2] is based on two discoveries: (1) the connection between bivalent Boolean logic and the algebra of quaternions $\mathbb{H}$ [42]; (2) a natural closed Friedmann-Lemaître-Robertson-Walker (FLRW) metric on a quaternionic ray (as the Lorentzian metric generated by the translations of the natural Minkowski scalar product [42] along the left (right) invariant vector fields on the Lie group of nonzero quaternions [43]). The first result singles out the quaternion algebra as a model of a perceptible environment for an observer with Boolean logic, the second makes the whole framework GR-Friendly [42].

The fundametal object of HHQM is a quaternionic ray $\mathbb{H}^*$(called a *possible world*), representing a state of a physical system (analogous to the complex ray of the standard quantum mechanics).
With the two key results, each quaternionic ray has the following properties:
a) it is the set of nonzero quaternions;
b) it is a locally compact Lie group, under quaternion multiplication;
c) it is automatically endowed with a bi-invariant Haar measure generated by the group multiplication;
d) it is a smooth real four dimensional manifold;
e) it has a natural closed FLRW metric induced by quaternion algebra operations [43];
f) it has a Lebesgue measure induced by the FLRW metric;

g) visually it looks like an hourglass (embedded in a higher-dimensional Minkowski space), flaring toward Past and Future, with the "waist" three-sphere containing the identity of the Lie group.
h) it has two sets of preferred nonmetric directions (*vistas*), along the integral curves of the left and right invariant vector fields.
Thus, within the HHQM kinematics, a state of a system can be also interpreted as a copy of spacetime and hence as the *cosmology* of the system's "residence".
HHQM utilizes quaternionic *Antihermitian* operators with quadruples of real numbers as eigenvalues.

3. HHQM Dynamics

The dynamics of HHQM is a (nonstandard) generalization of the Kähler bundle dynamics of geometric formulations of complex quantum mechanics [5,6,8,10,15,18,28,29,30,48]. More specifically, it is now a Hyperkähler bundle with $\mathbb{H}^*$ as its fiber, and three symplectic structures instead of one [17]. In other words, the dynamics is represented by a superposition of three Hamiltonian flows on the Hyperkähler bundle, who's fiber is a diffeomorphic copy of spacetime (possible world), each with a closed FLRW metric parameterized by the scale factor. The Riemannian part of the Hyperkähler structure is called the *propensity metric* of the system. It's main function is to measure geodesic distance between fibers, which is the basis for the measurement procedure in HHQM. The standard complex quantum mechanics (with *Antihermitean* operators) is a *degenerate* case of HHQM: two out of four dimensions are collapsed in each possible world, which destroys most of the structures described above.

Recalling that states in HHQM (as mathematical entities) are diffeomorphic copies of spacetime, we can interpret a physical system in HHQM as a *fine-graining* of the cosmology of it's "residence". Intuitively, every physical system is the whole spacetime plus some extra structures.

Since only the closed FLRW (smooth and nondegenerate everywhere) metric appears in any physical configuration, HHQM is singularity-free kinematicaly. This metric is relatively simple, yet the dynamics is enormously rich due to the sophisticated transverse geometry of the Hyperkähler bundle across fibers, and singularity-like structures (caustics, bifurcations, etc.) can be encountered dynamically.

However, because of the absence of true singularities, HHQM does not need full Einstein Field Equations, and the main dynamical variable in HHQM is the propensity metric. But of course, we use GR perturbation theory as an effective phenomenological bridge. The Three Fundamental Axioms of GR (Four Dimensionality, Manifold Structure and Metric Signature) are no longer ad hoc in this approach, and appear automatically. Thus, being GRfriendly, HHQM is however dynamically independent of GR. Kinematical singularity avoidance raises hopes that renormalization-like procedures will be unnecessary in HHQM-based field theories, although it remains an open technical problem.

4. HHQM Semantics

HHQM is Observer-centric, and the major part of the original paper is dedicated to rigorous definitions of the notion of an Observer, his logic and related concepts [42,44,45]. It starts with the most primitive, undefined entities of the framework (*elementary experiences*) "observations" and "actions", and culminates in the definitions of an Experient (an Observer with certain logic), the *Home paradigm, perception domain,* several notions of time, spacetime, physical systems, etc. The key result is that the Home paradigm of an Observer with bivalent Boolean logic is isomorphic to the quaternion algebra $\mathbb{H}$, with two *consistent* (matching his logic) subparadigms $\mathbb{C}$ and $\mathbb{R}$, of complex and real numbers, respectively [42,44]. We briefly discuss possible connections between the three paradigms, their internal symmetry groups $SU(2)$, $U(1)$ and $\mathbb{Z}_2$ and three generations of matter in Section 8.

As with any theory of a similar level of structure, there are several plausible versions of semantics. This approach uses some aspects of Leibniz's "Possible Worlds" ontology [31]. We call the total space of the Hyperkähler bundle the *monocosm* (the set of all possible configurations of the system), and each fiber a *possible world.* The system is thought of as moving through the bundle along the Hyperhamiltonian flow, *marking possible worlds* as it's *instantaneous fine-grainings.* This natural interpretation is conceptually clear, but stops working in the standard QM. The measurement procedure involves (see [44,45] for details) two possible worlds (the *source* and the *target* worlds), the inverse geodesic distance between them (propensity of the measurement, supplied by the propensity metric) and a quaternionic regular map f (the *observable* of the measurement). The shorter the geodesic distance between the worlds, the more likely that the system ends up in the target world as a result of the measurement. It also invokes the notion of accessibility of possible worlds: *f-accessible* worlds correspond to eigenstates (called *f-proper states*). A measurement is considered *successful* only if the target possible world is accessible, in which case it becomes the *actual world* of the measurement. It should be stressed that conceptually the measurement mechanism of HHQM is radically different from (and independent of) the Born rule-based procedures of the standard complex QM, and full derivation of connections between the two formalisms remains an open problem [46]. One of the goals of this work is to attract the wider quantum community's attention to this and some related problems.

5. Two-Measure Framework and the Origin of Matter

We adopt the two-measure approach where along with a spacetime metric-induced Lebesgue measure, a Haar measure associated with the underlying configuration-space degrees of freedom is used. Two-measure structure has a natural interpretation: while the standard Lebesgue measure λ takes care of matter/radiation density, the Haar measure μ, as purely internal spacetime, assumes responsibility for vacuum energy density [19-26].

The FLRW scale factor a connects the temporal evolution to the radial structure. Near the origin in canonical coordinates the spherical coordinate $\chi \to \pi/2$ (equatorial limit) and $a\ (\eta) \to 0$ as the cosmological scale collapses. This gives three natural regimes:

Regime I — Cosmological scale ($r \sim 1$, far from origin): the Haar and Lebesgue measures are comparable. The density r^{-4} is O(1), and Haar measure closely tracks the FLRW volume element.

Regime II — Intermediate ($r \ll 1$ but $r > 0$): the density r^{-4} grows rapidly. Haar measure overweights small-r regions enormously relative to Lebesgue. For $q \in \mathbb{H}$, a ball $B_\epsilon = \{|\ q\ |< \epsilon\}$:

$$\mu(B_\epsilon \cap \mathbb{H}^\circ) = \int_0^\epsilon \frac{r^3}{r^4} \cdot (\text{angular factor})\, dr = C \int_0^\epsilon r^{-1} dr = C \ln(1/\epsilon) \to \infty$$

Where C is a normalization constant. So μ is not finite near the origin — it diverges logarithmically. This is the first critical asymmetry. Regime III — The origin itself ($r = 0$): it is excluded from $\mathbb{H}^\circ$ by construction. Lebesgue assigns it measure zero; Haar cannot even be evaluated there. The origin acts as a measuretheoretic singularity that is simultaneously: (a) kinematically forbidden (outside spacetime); (b) a Lebesgue-null set; (c) a Har-divergence point. A mascon (mass concentration) in the classical sense is a region where the local energy density exceeds the surrounding average without being supported by ordinary matter. In HHQM framework mascons are concentrations of vacuum Har-measure excess, with no underlying material substrate. From the density $d\mu/d\lambda = r^{-4}$, consider the competition between Haar weight and Lebesgue volume for a thin shell $S_\epsilon = \{r \in (\epsilon, 2_\epsilon)\}$:

$$\lambda(S_\epsilon) \sim \epsilon^4, \mu(S_\epsilon) \sim \int_\epsilon^{2\epsilon} r^{-1} dr = \ln 2; (\text{independent of } \epsilon!)$$

This scale-invariance of $\mu(S_\epsilon)$ follows from the Haar invariance; every logarithmic shell carries equal Haar weight regardless of its radius. There is no Haar-preferred scale near the origin. A mascon's effective radius must therefore emerge from somewhere else — from the interplay of Haar measure with the additional structure the physical system imposes. The natural candidate is the propensity metric g. Near the origin, the FLRW scale factor $a \to 0$, so g degenerates spatially. The competition between the Haar divergence r^{-4} and the metric degeneracy $a^2 \to 0$ produces a balance condition. For a physical system, the propensity is $g(\phi,\psi) = d^{-1}$ where d is the propensity-metric geodesic length. The Haar-weighted geodesic distance between two states at radii r_1, r_2 near the origin, along a radial path, is:

$$d_\mu(r_1, r_2) = \int_{r_1}^{r_2} \sqrt{\frac{d\mu}{d\lambda}} \cdot \sqrt{g_{rr}}\, dr = \int_{r_1}^{r_2} r^{-2} \cdot a(\eta(r))\, dr$$

where we used $\sqrt{r^{-4}} = r^{-2}$ and $\sqrt{g_{rr}}$ and √grr pulls in the FLRW scale factor. Near the origin, writing where we used r $a \sim a_0 r^\beta$ for some power β (dictated by the cosmological evolution), this becomes:

$$d_\mu \sim a_0 \int_{r_1}^{r_2} r^{\beta-2}\, dr$$

The critical case is $\beta = 1$, giving $d\mu \sim a_0 \ln(r_2/r_1)$ — logarithmically divergent; $\beta > 1$, the integral converges to a finite value as $r_1 \to 0$, meaning the origin is at finite geodesic distance. The transition at $\beta = 1$ defines an effective radius:

$$r_{\text{eff}} \sim \frac{1}{a_0}$$

Below this scale, the Haar-weighted geodesic distance saturates — states closer than reff to the origin become indistinguishable in propensity terms. This is the particle-like core, the mascon.

6. Universal Crossover Scale and Visibility Kernel

In HHQM the configuration space of each possible world is the Lie group $\mathbb{H}^{*} \cong \mathbb{R}^{+} \times S^{3}$ with bi-invariant Haar measure dμ. In radial coordinates the radial part of the Haar density behaves as $d\mu/dr \propto r^{-4}$. The cumulative Haar excess inside a ball Br (normalized) is

$$\mu(B_r) \propto \int_0^r s^{-1}\,\mathrm{d}s = \ln(1/r).$$

The Lebesgue volume is $\lambda(B^{r}) \propto r^{4}$. The dimensionless ratio

$$\Delta(r) := \frac{\mu(B_r)}{\lambda(B_r)} \sim \frac{\ln(1/r)}{r^4} \cdot r^4 = \ln(1/r)$$

quantifies the relative dominance of structural (Haar) vs. metric (Lebesgue) measure. This grows without bound as $r \to 0$, but slowly (logarithmically). The crossover scale r^{*} is uniquely defined as the point where the two measures balance ($\Delta(r^{*}) = 1$), i.e., the solution to $\ln(1/r^{*}) = 1$:

$$r^* = e^{-1} \approx 0.367879.$$

This value is structurally forced by the logarithmic nature of the Haar measure on the multiplicative group $\mathbb{R}^{+}$ (the radial factor of $\mathbb{H}^{*}$) and is independent of dimension (see paradigms in Sec. 8). Uniqueness follows because the logarithm is the unique scale-invariant function under the group action; no other solution satisfies the balance without free parameters. Higher-order propensity weighting yields only $O(\delta)$ corrections.

The visibility kernel quantifies the observable coupling—the finite overlap region where both Haar (structural/vacuum) and Lebesgue (metric/matter) measures contribute comparably while the propensity metric remains non-degenerate. It is uniquely determined as the normalized transition function between the two regimes. The observable (baryonic/luminous) density is the propensity weighted geometric mean of the two measures in the transition zone $x = \chi/\chi_s \approx 1$:

$$\rho_{\text{visible}} \propto \sqrt{\rho_{\text{Haar}} \cdot \rho_{\text{Lebesgue}}} \times \text{propensity factor}.$$

Near the crossover the propensity saturates as $\sim 1/(1 + x)^{2}$ (from geodesic distance in the degenerating FLRW metric). The radial weighting in comoving coordinates supplies the linear prefactor x. Normalizing so that $\int_0^\infty \Sigma(x)\rho_{\text{DM}}(x)\,\mathrm{d}x$ reproduces the observed baryon fraction while ensuring smoothness and $\Sigma(0) = \Sigma(\infty) = 0$ yields the unique closed-form solution

$$\Sigma(x) = \frac{x}{(1+x)^2}.$$

This is the exact solution to the first-order ODE describing balanced overlap

$$\frac{\mathrm{d}\Sigma}{\mathrm{d}x} = \Sigma(x)\frac{1-2x}{1+x},$$

with boundary conditions $\Sigma(0) = 0$, $\Sigma(\infty) = 0$, and peak at the crossover $x = 1$. The form is not ad hoc—it is the minimal rational function enforcing the Haar–Lebesgue balance, propensity suppression, and volume-element weighting required by HHQM kinematics. The unified kernel is then $K(x) = \Sigma(x) \bullet \Pi_{\text{time}}$ with $\Pi_{\text{time}} = 1/2$, the Arrow of Time Projection.

For $r > r^{*}$: Lebesgue and Haar are comparable, extended field-like behavior. For $r < r^{*}$: Haar strongly dominates, propensity suppressed, localized behavior.

Summarizing, a mascon is a region of $\mathbb{H}^{*}$ where:

(a) Measure imbalance

$$\Delta(r) = \frac{\mu(B_r)}{\lambda(B_r)} \gg 1$$

(b) Propensity saturation $g \to 0$ as $r \to 0$

(c) Finite observable coupling

$$\Sigma(x) \neq 0, x \sim 1$$

Intuitively, (a) deep inside (pure Haar) → Dark Sector; (b) outside (pure Lebesgue) → Classical Fields; (c) at the boundary → Luminous Sector, observable particles.

This crossover r^* is universal within the HHQM framework — it depends only on the group structure of $\mathbb{H}^*$, not on the specific physical system. It represents a natural Compton-scale analogue: below r^*, the system cannot be resolved as extended by any measurement (successful f-observation) because the propensity to reach worlds inside r^* is exponentially small.

7. Mascons, Topological Quantization

From [43] Definition 6.2, (u,a)-vistas are integral curves of left-invariant vector fields on H^*, computed explicitly in equation (23):

$$w(t) = e^{u^0 t}\left(\frac{-u^1\bar{x} - u^2\bar{y} - u^3\bar{z}}{\omega}\sin\omega t + \bar{w}\cos\omega t\right)$$

with $\omega = \sqrt{(u^1)^2 + (u^2)^2 + (u^3)^2}$.

Near the origin, $\bar{w}\bar{x}\bar{y}\bar{z} \to 0$. The vistas degenerate — their oscillatory S^3 component (frequency ω) survives while the radial envelope $e^{u^0 t}\cdot r \to 0$. What persists is a pure rotational structure with no translational extent: the vista winds around the S^3 fiber at fixed, vanishing radius.

This is precisely particle-like: an object with internal angular structure (the S^3 winding, ω) but no spatial extension in the Lebesgue sense. The effective radius reff marks the scale below which the translational degrees of freedom are Haar-suppressed and only the internal $SU(2)$ structure of $\mathbb{H}^* \cong SU(2) \times \mathbb{R}^+$ remains dynamically relevant.

The quantity ω then plays the role of an internal frequency — an intrinsic property of the particle-like object unrelated to its position, analogous to spin or rest-mass frequency. From the vista equations, ω is invariant under rescaling r → λr (it depends only on the direction $u/\mid u\mid$), confirming it as a purely internal quantum number.

From Definition 9.4, an *f*-observation is successful only if the target world *W* is *f*-accessible — there must exist an f-proper state there [44]. Near the origin, the *f*-proper states are vertical in the bundle w.r.t. the propensity metric. As $a \to 0$, the world W has a metric degenerating in spatial directions. The verticality condition becomes increasingly easy to satisfy — almost any state near the origin is f-proper because the spatial tangent space is metrically collapsed.

This means (a) near the origin: many accessible worlds, but all with near-zero propensity; (b) away from origin: fewer accessible worlds, but finite propensity. A region where accessible worlds proliferate remains unreachable — a Haar-measure shadow of high internal structure with vanishing external propensity. The measurement can confirm the mascon's existence (many f-proper states) but not its location (propensity → 0), which is analogous to quantum indeterminacy. Define the Haar mass of a mascon centered at scale $r_0 < r^*$ as:

$$M(r_0) := \int_{B_{r_0}} \frac{d\mu}{d\lambda}\cdot\rho_{\mathrm{vac}}\,d\lambda = \rho_{\mathrm{vac}}\int_0^{r_0} r^{-4}\cdot r^3\,dr = \rho_{\mathrm{vac}}\int_0^{r_0} r^{-1}\,dr = \rho_{\mathrm{vac}}\ln(1/r_0)$$

A mascon configuration determines a continuous map

$$\mathcal{Q} : S^3 \to S^3.$$

Since homotopy classes of Q are characterized by

$$\pi_3(S^3) = \mathbb{Z},$$

the configuration possesses an integer topological charge

$$\mathbf{Q} = \deg(\mathcal{Q}) \in \pi_3(S^3).$$

The Haar mass of a mascon is proportional to this charge,

$$M = M_0|\mathbf{Q}|,$$

where M_0 is a constant (interpreted as the fundamental Haar mass scale). Consequently the mascon spectrum is quantized,

$$M_n = nM_0, \qquad n = 1, 2, 3, \ldots$$

and the integer shell number is identified with the topological degree n = |Q|. Discrete mass values correspond to discrete radii:

$$r_n = e^{-n}, M_n = n \cdot \rho_{\text{vac}}, \quad n = 1, 2, 3, \ldots$$

The mass spectrum is linear in n with a universal spacing ρvac = const — it follows from the logarithmic shell-equivalence of Haar measure established earlier. The quantum number n counts the number of Haar-equivalent shells enclosed within the mascon, which maps naturally onto the internal SU(2) winding structure of the S^3 fiber.

The connection to the vista frequency ω from [43] equation (23) is then:

$$\omega_n \sim e^n \cdot \omega_0,$$

where ω_0 is a constant.

Internal frequency grows exponentially with the shell number n while Haar mass grows linearly — meaning heavier mascons oscillate faster internally, which is consistent with the relativistic $E = mc^2$ identification of rest mass with internal frequency.

Each paradigm $\mathbb{R} \subset \mathbb{C} \subset \mathbb{H}$ carries its own Haar measure. The Haar–Lebesgue density for each: H-paradigm:

$$\frac{d\mu_H}{d\lambda_4} = r_H^{-4},$$

crossover at $rH^* = e^{-1}$

$\mathbb{C}$-paradigm: Perception domain $C^* \cong \mathbb{R}^2 \setminus \{0\}$, Haar measure $d\mu C = r^{-2} d\lambda 2$, so:

$$\frac{d\mu_C}{d\lambda_2} = r^{-2}, \Delta_C(r) = \ln(1/r), r_C^* = e^{-1}$$

$\mathbb{R}$ -paradigm: Perception domain $\mathbb{R}^* \cong \mathbb{R} \setminus \{0\}$, Haar measure $d\mu_R = r^{-1} d\lambda 1$, so:

$$\frac{d\mu_R}{d\lambda_1} = r^{-1}, \Delta_R(r) = \ln(1/r), r_R^* = e^{-1}$$

Remarkably, all three crossover scales are e^{-1} in their respective units — the logarithmic crossover condition $\Delta = 1$ gives $r^* = e^{-1}$ regardless of dimension. This is structurally forced by the logarithmic nature of Haar measure on $\mathbb{R}^+$ in all cases.

The radial part of the Haar measure, $d\mu_r \propto r^{-1} dr$, is identical for all three paradigms, giving the same radial integral:

$$\int_0^{r^*} r^{-1}\, dr = 1.$$

However, the mass scales differ because the Haar excess integrated over the mascon differs. The angular volumes of the internal symmetry groups differentiate the masses:

$$M^H \sim \rho_{\text{vac}} \left(\int_0^{r^*} r^{-1}\, dr \right) \cdot \text{Vol}(S^3) = \rho_{\text{vac}} \cdot 1 \cdot 2\pi^2,$$

$$M^C \sim \rho_{\text{vac}} \left(\int_0^{r^*} r^{-1}\, dr \right) \cdot \text{Vol}(S^1) = \rho_{\text{vac}} \cdot 1 \cdot 2\pi,$$

$$M^R \sim \rho_{\text{vac}} \left(\int_0^{r^*} r^{-1}\, dr \right) \cdot \text{Vol}(\{\pm 1\}) = \rho_{\text{vac}} \cdot 1 \cdot 2.$$

This hints on a possibility that three consistent paradigms $\mathbb{R} \subset \mathbb{C} \subset \mathbb{H}$ correspond to three matter generations.

8. Angular Content and the Mass Hierarchy Ansatz

Thus, for a mascon at shell number *n*,
$\mathbb{H}$ -paradigm, internal group *SU*(2):

$$M_n^H = n \cdot \text{Vol}(S^3) \cdot \rho_{\text{vac}} = 2\pi^2 n \cdot \rho_{\text{vac}}$$

$\mathbb{C}$-paradigm, internal group U(1):

$$M_n^C = n \cdot \mathrm{Vol}(S^1) \cdot \rho_{\mathrm{vac}} = 2\pi n \cdot \rho_{\mathrm{vac}}$$

$\mathbb{R}$ -paradigm, internal group $\mathbb{Z}_2$:

$$M_n^R = n \cdot \mathrm{Vol}(\{+1, -1\}) \cdot \rho_{\mathrm{vac}} = 2n \cdot \rho_{\mathrm{vac}}$$

The mass ratios between paradigms at the same shell number n are:

$$M^H : M^C : M^R = 2\pi^2 : 2\pi : 2 = \pi^2 : \pi : 1$$

This is a purely geometric ratio determined by the volumes of S^3, S^1, and S^0 — the unit spheres in $\mathbb{R}^4$, $\mathbb{R}^2$, $\mathbb{R}^1$ respectively. This gives a hierarchical mass spectrum with the $\mathbb{H}$ -paradigm heaviest, C intermediate, and R lightest. Each paradigm's internal symmetry group generates its own vista structure. The charges of mascons in each generation should correspond to representations of these groups.

$\mathbb{R}$ -paradigm, internal group $\mathbb{Z}_2$: Only one nontrivial representation: the sign representation. This gives a single binary quantum number — electric charge ±e in appropriate units.

$\mathbb{C}$-paradigm, internal group $U(1)$: Representations labeled by integer winding numbers $m \in \mathbb{Z}$. This generates a continuous charge spectrum restricted to integers. The second generation carries the same charges as the first but with additional $U(1)$ structure from the C-paradigm, manifesting as heavier masses (the π factor) without new charge quantum numbers.

$\mathbb{H}$-paradigm, internal group $SU(2)$: Representations labeled by j = 0,1/2,1,3/2,... generate non-Abelian charge structure. The third generation carries full $SU(2)$ representation content, manifesting as both the heaviest masses (π^2 factor) and the richest internal symmetry.

The $\mathbb{R}$-paradigm is particularly interesting for neutrinos. Its internal group is $\mathbb{Z}_2$ with no continuous representations — neutrinos in this paradigm carry no continuous charge quantum numbers. The only quantum number is the$\mathbb{Z}_2$ sign, which can be interpreted as chirality (left/right handedness).

The $\mathbb{R}$-paradigm Haar mass for neutrinos:

$$M_\nu^R = 2n \cdot \rho_{\mathrm{vac}}$$

is the smallest possible Haar mass — just the $\mathbb{Z}_2$ angular factor with no π or π^2 enhancement. This naturally produces hierarchically light neutrino masses compared to charged leptons, without a seesaw mechanism. The ratio of electron mass to electron neutrino mass is:

$$\frac{M_e}{M_{\nu_e}} \sim \frac{2\pi}{2} = \pi$$

at the same shell number — a factor of π suppression for the neutrino, arising from the $U(1)$
versus $\mathbb{Z}_2$ angular content.

Furthermore, since $\mathbb{R}^* \cong \mathbb{Z}_2 \times \mathbb{R}^+$ has a discrete internal group, the neutrino of the R -paradigm has no continuous internal rotation — it cannot carry angular momentum in the standard sense. This resembles the Majorana nature of neutrinos: a particle whose internal group is $\mathbb{Z}_2$ is its own antiparticle (the sign flip +1 → −1 is the only nontrivial group. Matter-antimatter distinction in our framework is *topological charge sign, together with vista chirality* (not either separately: left/right vistas correspond to two chiralities of the internal $SU(2)$ structure; topological charge sign determines the orientation of S^3 winding).

9. Dark Matter Profile

We start from the NFW-Einasto inspired dark matter density profile [16,35] modified for the HHQM two-measure framework

$$\rho_{\mathrm{DM}}(\chi) = \frac{C}{\chi(\chi + \chi_s)^3},$$

where χ is the comoving radial coordinate, $\chi_s = r^*/a(\eta)$ is the crossover scale, and $r* = e^{-1}$ is the universal crossover from the group structure of $\mathbb{H}^*$, C is a normalization constant.

Citation: Trifonov, V., Trifonov, P. V. (2026). On Geometric Origin of Dark Matter, Dark Energy, and the Fine-Structure Constant. *J Theor Phys Math, 4*(4), 1-17.

The visibility kernel quantifying the overlap between the Lebesgue (metric) measure and the Haar (structural) measure is

$$\Sigma(x) = \frac{x}{(1+x)^2}; x = \frac{\chi}{\chi_s}.$$

The baryonic (observable) density is postulated to be the dark matter density weighted by this kernel and a dimensionless constant κ:

$$\rho_b(\chi) = \kappa\,\Sigma(x)\,\rho_{\mathrm{DM}}(\chi).$$

Substitute the expressions for $\Sigma(x)$ and ρ_{DM}:

$$\rho_b(\chi) = \kappa \cdot \frac{x}{(1+x)^2} \cdot \frac{C}{\chi(\chi+\chi_s)^3}.$$

Now express everything in terms of x and χ_s:

$$\chi = x\chi_s, \qquad \chi + \chi_s = \chi_s(1+x).$$

Thus

$$\rho_b(\chi) = \kappa \cdot \frac{x}{(1+x)^2} \cdot \frac{C}{(x\chi_s)\cdot\big(\chi_s(1+x)\big)^3}.$$

Simplify step by step:

$$(x\chi_s)\cdot\big(\chi_s(1+x)\big)^3 = x\chi_s \cdot \chi_s^3(1+x)^3 = x\chi_s^4(1+x)^3.$$

Therefore

$$\rho_b(\chi) = \kappa \cdot \frac{x}{(1+x)^2} \cdot \frac{C}{x\chi_s^4(1+x)^3} = \kappa \cdot \frac{C}{\chi_s^4} \cdot \frac{x}{x} \cdot \frac{1}{(1+x)^2(1+x)^3}.$$

Cancelling x and combining the (1 + x) factors:

$$\boxed{\rho_b(\chi) = \kappa\frac{C}{\chi_s^4}\frac{1}{(1+x)^5}}.$$

The proper volume element in comoving coordinates (on a spatial slice of the closed FLRW metric, working in the small-χ / nearly-flat approximation for integration near the crossover) is

$$dV = 4\pi\chi^2 d\chi.$$

Hence

$$M_b^{\mathrm{total}} = \int_0^\infty \rho_b(\chi)\,4\pi\chi^2 d\chi = 4\pi\kappa\frac{C}{\chi_s^4}\int_0^\infty \frac{\chi^2}{(1+\chi/\chi_s)^5}d\chi.$$

Change variables: $x = \chi/\chi_s$, so $\chi = x\chi_s$, $d\chi = \chi_s dx$, and $\chi^2 d\chi = x^2\chi_s^3 dx$:

$$M_b^{\mathrm{total}} = 4\pi\kappa\frac{C}{\chi_s^4}\cdot\chi_s^3\int_0^\infty \frac{x^2}{(1+x)^5}dx = 4\pi\kappa\frac{C}{\chi_s}\int_0^\infty \frac{x^2}{(1+x)^5}dx.$$

Let

$$I = \int_0^\infty \frac{x^2}{(1+x)^5}dx.$$

Substitute $u = 1 + x$, so $x = u - 1$, $dx = du$, and when $x = 0$, $u = 1$; when $x \to \infty$, $u \to \infty$:

$$I = \int_1^\infty \frac{(u-1)^2}{u^5} du = \int_1^\infty \frac{u^2 - 2u + 1}{u^5} du = \int_1^\infty \left(u^{-3} - 2u^{-4} + u^{-5}\right) du.$$

Integrate term by term:

$$\int_1^\infty u^{-3} du = \left[\frac{u^{-2}}{-2}\right]_1^\infty = 0 - \left(-\frac{1}{2}\right) = \frac{1}{2}.$$

$$\int_1^\infty -2u^{-4} du = -2\left[\frac{u^{-3}}{-3}\right]_1^\infty = -2\left(0 - \left(-\frac{1}{3}\right)\right) = -2 \cdot \frac{1}{3} = -\frac{2}{3}.$$

$$\int_1^\infty u^{-5} du = \left[\frac{u^{-4}}{-4}\right]_1^\infty = 0 - \left(-\frac{1}{4}\right) = \frac{1}{4}.$$

Sum:

$$I = \frac{1}{2} - \frac{2}{3} + \frac{1}{4} = \frac{6}{12} - \frac{8}{12} + \frac{3}{12} = \frac{1}{12}.$$

Therefore

$$M_b^{\text{total}} = 4\pi\kappa \frac{C}{\chi_s} \cdot \frac{1}{12} = \boxed{\kappa \frac{\pi C}{3\chi_s}}.$$

$$\frac{\Omega_{\text{DM}}}{\Omega_b} = \frac{M_{\text{DM}}^{\text{total}}}{M_b^{\text{total}}} = \frac{\frac{2\pi C}{\chi_s}}{\kappa\frac{\pi C}{3\chi_s}} = \frac{2\pi C}{\chi_s} \cdot \frac{3\chi_s}{\kappa\pi C} = \frac{6}{\kappa}. \tag{1}$$

Thus, HHQM predicts about six times more dark matter than luminous. The dark matter distribution represents mascons with net zero topological charge (bound states of matter-antimatter configurations), hence this abundance ratio is interpreted as the total Haar-mascon abundance before imposing charge neutrality and visibility constraints. The actual abundance ratio should be smaller, and the finer adjustment (O(1)) is controlled by κ which in the HHQM framework could be a function (not a mere constant) of the theory's "soft" parameters (the crossover scale, propensity, etc.), that affect charge neutrality and visibility constraints. Computation of the exact functional form of κ from within HHQM remains an open problem.

10. Modified Background Cosmology and Linear Perturbations

The spacetime geometry is the standard closed FLRW metric in conformal time η:

$$ds^2 = a(\eta)^2\left[-d\eta^2 + d\Omega_3^2\right],$$

where $d\Omega_3^2$ is the metric on the unit three-sphere S^3 and the comoving curvature parameter is $k = +1$.

The left-Haar measure on the Lie group $\mathbb{H}^*$ is bi-invariant. Consequently, the three-volume of any spatial slice obtained by left (or right) translation of the unit "waist" three-sphere is independent of the scale factor $a(\eta)$. Associating a fixed total vacuum energy E_{vac} with this Haar three-volume yields a constant physical energy density:

$$\rho_{\text{Haar}} \equiv \frac{E_{\text{vac}}}{V_{\text{Haar}}} = \rho_{m0} = \text{constant}.$$

(Ordinary matter/radiation densities are measured with respect to the Lebesgue volume form induced by the FLRW metric and therefore scale as $\rho_m \propto a^{-3}$). In other words, matter/radiation density rapidly decreases, while the vacuum energy density (being constant) catches up and eventually overtakes it, producing accelerated expansion geometrically.

Thus, *the observed cosmological constant is not the sum of all vacuum fluctuations* — it is the Haar–Lebesgue mismatch at the single crossover scale r^*, concentrated there by the group structure of $\mathbb{H}^*$. The 10^{123} discrepancy arises because *Lebesgue integration in QFT sums this mismatch over all scales from r^* down to the Planck length,* each contributing $\mathcal{O}(1)$ in Haar terms, but $\mathcal{O}(r^{-4})$ in Lebesgue terms — an integral that diverges as $\ln(r^*/r_{\text{Planck}}) \sim 123\ln(10)$.

The Einstein equations $G_{\mu\nu} = 8\pi G T_{\mu\nu}$ for the FLRW metric reduce to the first Friedmann equation (in cosmic time t): The corresponding effective pressure follows from the continuity equation $\dot{\rho} + 3H(\rho + P) = 0$:

$$P_{\mathrm{Haar}} = -\rho_{m0} \quad \Rightarrow \quad w_{\mathrm{eff}} = -1.$$

$$H^2 = \frac{8\pi G}{3}\rho - \frac{k}{a^2}, \qquad H \equiv \frac{\dot{a}}{a}.$$

Switching to conformal time via $dt = a d\eta$ gives $\dot{a} = a'/a = \mathscr{H}/a$ (where $\mathscr{H} \equiv a'/a$), (prime denotes derivative w.r.t. conformal time η) and

$$H = \frac{\mathscr{H}}{a} \quad \Rightarrow \quad \mathscr{H}^2 = \frac{8\pi G}{3}\rho\, a^2 - k.$$

Inserting $k = +1$ and the constant Haar vacuum density $\rho = \rho_{m0}$ produces the modified background equation:

$$\mathscr{H}^2 = \frac{8\pi G}{3}\rho_{m0}\, a^2 - 1. \tag{1}$$

In the late-time limit $a \gg 1$ this recovers pure de Sitter expansion:

$$\mathscr{H} \approx \sqrt{\frac{8\pi G \rho_{m0}}{3}}\, a, \qquad H \approx \mathrm{const} = \sqrt{\frac{8\pi G \rho_{m0}}{3}},$$

corresponding to an effective cosmological constant $\Lambda_{\mathrm{eff}} = 8\pi G_{\rho m0}$.

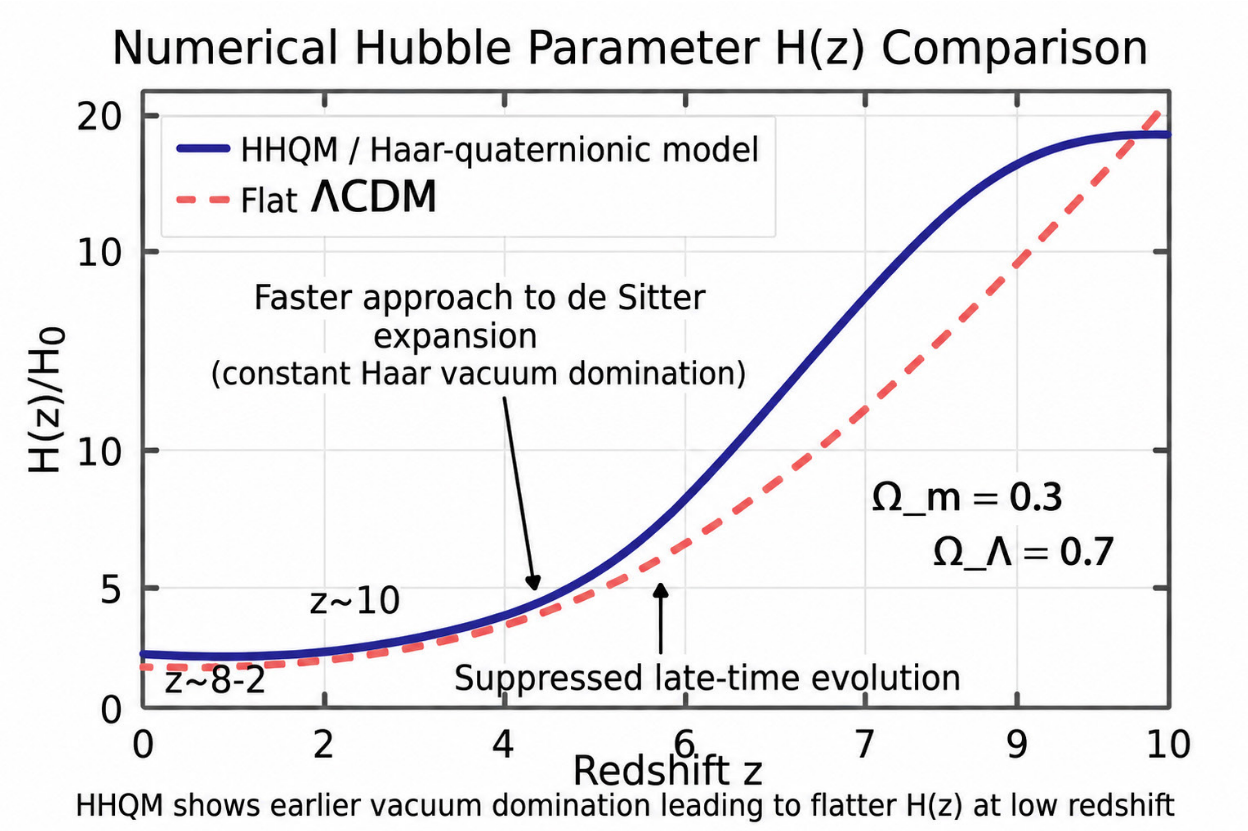

Figure 1: Numerical comparison of the Hubble parameter $H(z)/H_0$ as a function of redshift z. The solid blue line shows the HHQM (Haar-quaternionic) model with a constant vacuum energy density ρHaar arising from the bi-invariant Haar measure on the quaternionic ray $\mathbb{H}^{*}$. The dashed red line shows the standard flat ΛCDM cosmology with matter density parameter $\Omega_m = 0.3$ and dark-energy density parameter $\Omega_\Lambda = 0.7$. The HHQM model exhibits an earlier approach to de Sitter expansion (faster rise of $H(z)$ at moderate-to-high redshift) due to the constant Haar vacuum term in the modified Friedmann equation. At low redshift the HHQM curve becomes noticeably flatter, reflecting suppressed late-time evolution of the Hubble parameter. This behavior is a direct consequence of the frozen structure growth (δ_n plateau) discussed in the text and leads to lower $f\sigma_8(z)$ and S_8 values, consistent with current observational tensions. The plot is normalized to the same present-day value H_0

For the Newtonian (longitudinal) gauge on the closed FLRW background, the perturbed line element for a single hyperspherical-harmonic mode with eigenvalue $\mu = n^2 - 1$ ($n \geq 2$) is

$$ds^2 = a(\eta)^2\Big[-(1+2\Phi_n)d\eta^2 + (1-2\Psi_n)\gamma_{ij}\,dx^i dx^j\Big],$$

where γ_{ij} is the metric on the unit three-sphere and Φ_n,Ψ_n are the scalar potentials. For the effective vacuum fluid ($w = -1$) the anisotropic stress vanishes at linear order, implying $\Phi_n = \Psi_n$.

The linearized Einstein equations and the continuity equation for the density contrast

$$\delta_n \equiv \frac{\delta\rho_n}{\rho_{m0}}$$

yield, after expansion in hyperspherical harmonics and elimination of the velocity perturbation, the exact second-order master ODE (see standard references on closed-universe perturbations, e.g. [39]):

$$\delta_n'' + \mathscr{H}\,\delta_n' - \frac{3}{2}\frac{\mathscr{H}^2+1}{a^3}\delta_n = 0. \tag{2}$$

The coefficient $\frac{3}{2}(\mathscr{H}^2+1)/a^3$ follows directly from the background Friedmann relation (1):

$$\frac{3}{2}\frac{\mathscr{H}^2+1}{a^3} = \frac{4\pi G\rho_{m0}}{a}.$$

Thus the source term vanishes ∝ 1/a at late times, producing frozen growth $(\delta_n' \to 0)$ $f\sigma_8(z)$ at low redshift, as claimed [9,11,32,33,36,37,41].

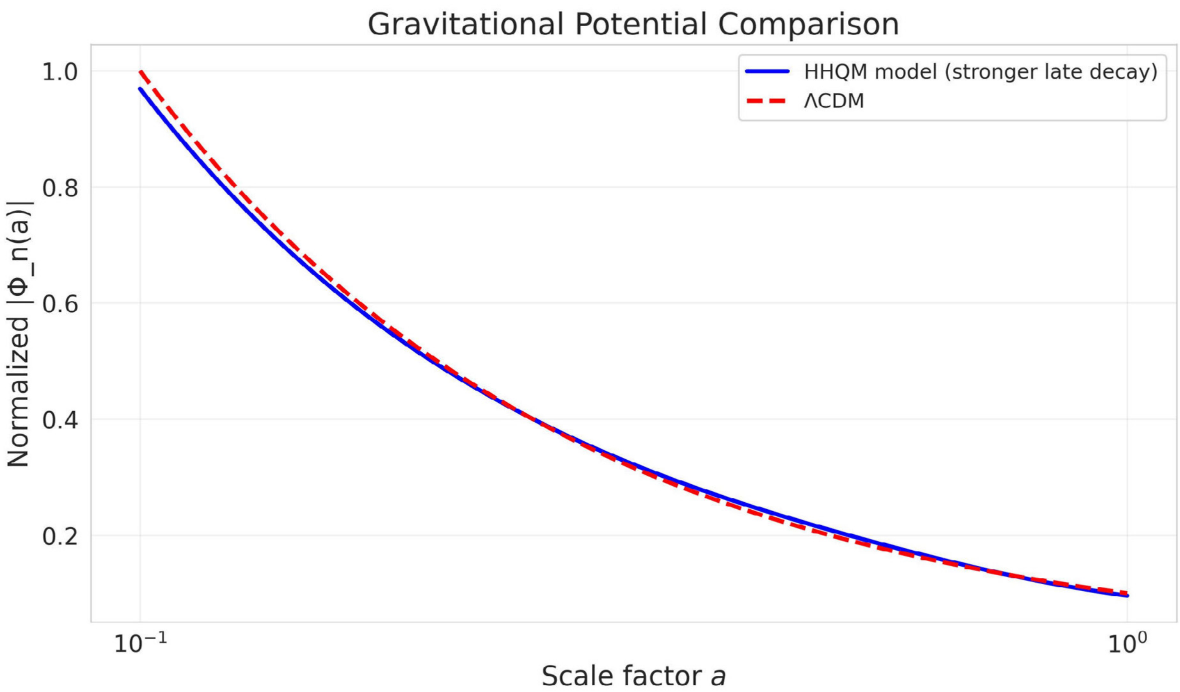

Figure 2: Normalized gravitational potential $|\Phi_n(a)|$ for the same mode. The solid blue line (HHQM model) exhibits stronger late-time decay compared to ΛCDM (dashed red), a direct consequence of earlier freezing of the density contrast δ_n. The difference remains within 10% for $0 < z < 2$, in agreement with current Stage-III data and testable with Stage-IV surveys (Euclid, Rubin, CMB-S4). This behavior implies reduced weak lensing amplitude and an enhanced Integrated Sachs-Wolfe (ISW) effect

11. Gravitational Potentials Φ_n for n>2

We now derive the algebraic relation between the Newtonian potential Φ_n and the density contrast δ_n. In Newtonian gauge, with vanishing scalar anisotropic stress, $\Phi_n = \Psi_n$, and the perturbed metric is

$$ds^2 = a^2(\eta)\left[-(1+2\Phi_n Q_n)d\eta^2 + (1-2\Phi_n Q_n)\gamma_{ij}dx^i dx^j\right],$$

Where Q_n is a scalar hyperspherical harmonic on the unit three-sphere,

$$\nabla^2 Q_n = -\mu Q_n, \qquad \mu = n^2 - 1, \qquad n > 2.$$

The linearized 00 Einstein equation in a closed FLRW background is

$$(\nabla^2 + 3)\Phi - 3\mathscr{H}(\Phi' + \mathscr{H}\Phi) = 4\pi G a^2 \delta\rho,$$

Where $\mathscr{H} = a'/a$. Expanding in Q_n gives

$$-(\mu - 3)\Phi_n - 3\mathscr{H}(\Phi_n' + \mathscr{H}\Phi_n) = 4\pi G a^2 \delta\rho_n.$$

Equivalently, with the sign convention chosen so that a positive overdensity corresponds to an attractive Newtonian potential,

$$(\mu - 3)\Phi_n + 3\mathscr{H}(\Phi_n' + \mathscr{H}\Phi_n) = -4\pi G a^2 \delta\rho_n.$$

For ordinary matter, the physical density scales with the Lebesgue volume,

$$\rho_m(a) = \frac{\rho_{m,*}}{a^3},$$

Where $\rho_{m,*}$ is a constant, so that

$$\delta\rho_n = \rho_m(a)\delta_n = \frac{\rho_{m,*}}{a^3}\delta_n.$$

Hence

$$4\pi G a^2 \delta\rho_n = \frac{4\pi G \rho_{m,*}}{a}\delta_n.$$

It is useful to define the matter source coefficient

$$S_m(a) \equiv 4\pi G a^2 \rho_m(a) = \frac{4\pi G \rho_{m,*}}{a}.$$

On scales where the potential evolves slowly compared with the Hubble drag term, or equivalently in the Newtonian/quasi-static limit, the term $3\mathscr{H}(\Phi_n' + \mathscr{H}\Phi_n)$ is subleading compared with the spatial Laplacian term. Therefore the Hamiltonian constraint reduces to the closed-space Poisson relation

$$(\mu - 3)\Phi_n \simeq -S_m(a)\delta_n.$$

This explicitly shows that the Newtonian potential is sourced by Lebesgue-measured matter perturbations rather than the Haar vacuum, which does not cluster at linear order. Hence, for $n > 2$

$$\boxed{\Phi_n \simeq -\frac{S_m(a)}{\mu - 3}\delta_n = -\frac{4\pi G \rho_{m,*}}{a(\mu - 3)}\delta_n.}$$

Thus the Newtonian potential has the standard cosmological scaling

$$\boxed{\Phi_n \propto \frac{\delta_n}{a}.}$$

12. Gravitational Potential Φ_2

In the simplified Poisson-like relation:

$$(\mu - 3)\Phi_n \simeq -S_m(a)\delta_n,$$

where $\mu = n^2 - 1$ and $S_m(a) = 4\pi G a^2 \rho_m(a)$, the left-hand side vanishes for $n = 2$ in this approximation, leading to an apparent singularity. The issue is that for the lowest scalar mode $n = 2$, the spatial Laplacian term does not dominate over the Hubble drag term, so the quasi-static approximation breaks down. We must use the full linearized 00 Einstein equation.

With zero anisotropic stress ($\Psi_n = \Phi_n$) and expanding in hyperspherical harmonics, the full constraint is:

$$-(\mu - 3)\Phi_n - 3\mathcal{H}(\Phi_n' + \mathcal{H}\Phi_n) = 4\pi G a^2 \delta\rho_n.$$

For $n = 2$, $\mu - 3 = 0$, leaving:

$$-3\mathcal{H}(\Phi_2' + \mathcal{H}\Phi_2) = 4\pi G a^2 \delta\rho_2.$$

The matter density perturbation is:

$$\delta\rho_2 = \rho_m(a)\,\delta_2, \qquad \rho_m(a) = \frac{\rho_{m,*}}{a^3},$$

where $\rho_{m,*}$ is a constant. Substituting:

$$-3\mathcal{H}(\Phi_2' + \mathcal{H}\Phi_2) = 4\pi G a^2 \cdot \frac{\rho_{m,*}}{a^3}\,\delta_2 = \frac{4\pi G \rho_{m,*}}{a}\,\delta_2.$$

Here $\mathcal{H} = a'/a$ (prime denotes derivative w.r.t. conformal time η).

We use $\frac{d}{d\eta} = a\mathcal{H}\frac{d}{da}$. hus:

$$\Phi_2' = a\mathcal{H}\frac{d\Phi_2}{da}.$$

The equation becomes:

$$-3\mathcal{H}\left(a\mathcal{H}\frac{d\Phi_2}{da} + \mathcal{H}\Phi_2\right) = \frac{4\pi G \rho_{m,*}}{a}\,\delta_2.$$

Factor $\mathcal{H}^2$:

$$-3\mathcal{H}^2\left(a\frac{d\Phi_2}{da} + \Phi_2\right) = \frac{4\pi G \rho_{m,*}}{a}\,\delta_2.$$

The background Friedmann equation (modified by the Haar measure) gives:

$$\mathcal{H}^2 = \frac{8\pi G}{3}\rho_{\text{vac}}a^2 - 1,$$

with ρ_{vac} constant. However, for the integration we keep $\mathcal{H}(a)$ general. Divide both sides by $-3\mathcal{H}^2$:

$$a\frac{d\Phi_2}{da} + \Phi_2 = -\frac{4\pi G \rho_{m,*}}{3a\mathcal{H}^2}\,\delta_2(a).$$

Notice the left-hand side is $\frac{d}{da}(a\Phi_2)$. Hence:

$$\frac{d}{da}(a\Phi_2) = -\frac{4\pi G \rho_{m,*}}{3}\,\frac{\delta_2(a)}{a\mathcal{H}(a)^2}.$$

Integrate from some initial scale factor a_i (where initial conditions are set) to a:

$$a\Phi_2(a) - a_i\Phi_2(a_i) = -\frac{4\pi G \rho_{m,*}}{3}\int_{a_i}^{a}\frac{\delta_2(\tilde{a})}{\tilde{a}\,\mathcal{H}(\tilde{a})^2}\,d\tilde{a}.$$

Thus the gravitational potential for $n = 2$ is:

$$\boxed{\Phi_2(a) = \frac{a_i}{a}\Phi_2(a_i) - \frac{4\pi G \rho_{m,*}}{3a}\int_{a_i}^{a}\frac{\delta_2(\tilde{a})}{\tilde{a}\,\mathcal{H}(\tilde{a})^2}\,d\tilde{a}.}$$

From their Eq. (2) for δ_n, the density contrast $\delta_2(a)$ freezes at late times to a constant $\delta_{2,\infty}$ because the source term decays as $1/a$.

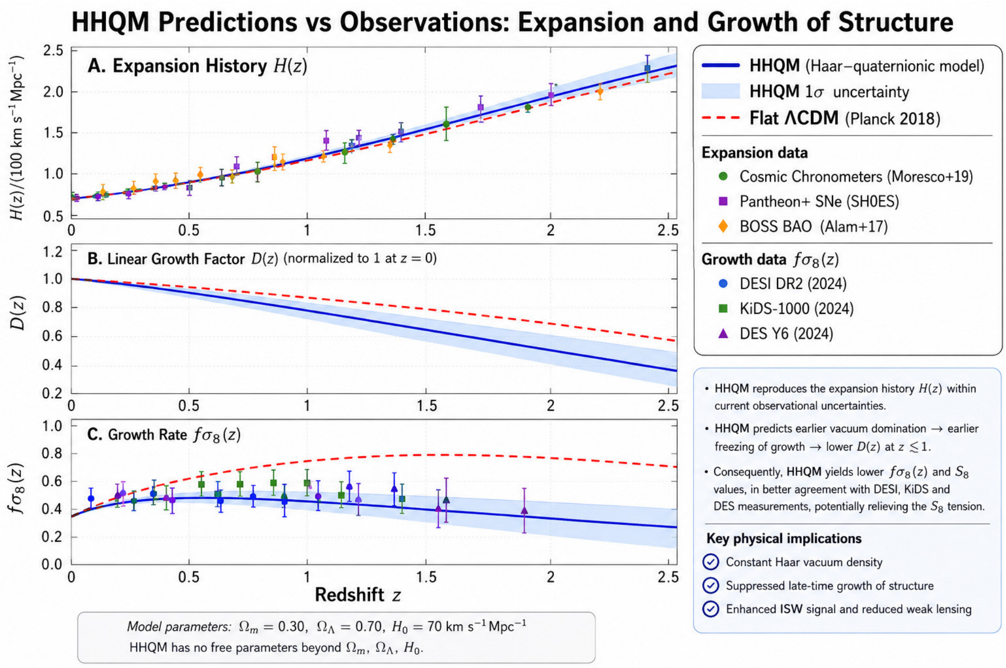

Figure 3: Comparison of the expansion and growth histories predicted by HHQM and the standard ΛCDM cosmology. While the background expansion remains broadly compatible with current observations, the two frameworks differ in their treatment of structure formation. The constant Haar-vacuum contribution in HHQM leads to an earlier transition toward vacuum domination, reducing the efficiency of late-time gravitational clustering. As a result, the model predicts lower growth amplitudes and weaker structure formation at recent epochs. These signatures provide direct observational tests with current and forthcoming large-scale-structure surveys

At late times, $\mathcal{H}^2 \approx \frac{8\pi G}{3}\rho_{\rm vac}a^2$ (de Sitter limit). Then:

$$\frac{\delta_2}{a\mathcal{H}^2} \approx \frac{\delta_{2,\infty}}{a \cdot \frac{8\pi G}{3}\rho_{\rm vac}a^2} = \frac{3\delta_{2,\infty}}{8\pi G\rho_{\rm vac}} \cdot \frac{1}{a^3}.$$

The integral $\int_{a_i}^{a} \tilde{a}^{-3} d\tilde{a}$ converges as $a \to \infty$ to a constant. Therefore:

$$a\Phi 2(a) \to \text{constant} \implies \Phi_2(a) \propto \frac{1}{a} \text{ at late times.}$$

The apparent singularity in the simplified Poisson equation for $n = 2$ is an artifact of dropping the time-derivative terms in the quasi-static approximation. The full constraint equation yields a regular, decaying potential.

Thus, in our model the late-time growth of δ_n freezes, so Φ_n decays approximately as a^{-1}. This is the same leading potential-decay law as in ΛCDM during dark-energy domination, with the observational difference residing in the detailed late-time growth history of δ_n. Earlier freezing of δ therefore implies faster decay of Φ, reduced weak-lensing amplitude, and an enhanced integrated Sachs-Wolfe (ISW) effect. These signatures — suppressed $f\sigma_8(z)$, reduced lensing, enhanced ISW — are testable with current DESI, Euclid, and Rubin Observatory data and provide clear falsification criteria [12].

13. HHQM and Fine-Structure Constant Ansatz

The same two-measure structure reappears at the microscopic level inside the monocosm fibers $\mathbb{H}^o$ [44]. These fibers are hourglass-shaped (time-symmetric under $t \mapsto -t$) but observed only along the directed temporal evolution field f^T. The observable electromagnetic sector is therefore the time-oriented projection of the full quaternionic structure.

$$\Pi_{\rm time} = \frac{1}{2}$$

The dimensionless coupling strength α arises as the total geometric volume of the internal symmetry space across the $U(1)$ charge space and the full $\mathbb{H}$ symmetry. The $U(1)$ charge space and the $SU(2)$ isospin space are not independent; they are related by the Hopf fibration $S^1 \hookrightarrow S^3 \to S^2$ (see e. g. [34]). The total geometric action for a $U(1)$ gauge field coupled to matter is the sum of the volumes of the total space, the base space and the fiber:

$$\alpha^{-1} = \mathrm{Vol}(S^1)\cdot\mathrm{Vol}(S^3) + \tfrac{1}{2}\mathrm{Vol}(S^3) + \tfrac{1}{2}\mathrm{Vol}(S^1).$$

The cross term Vol(S^1) • Vol(S^3) is the geometric realization of the *Hopf invariant* — the degree-1 generator of $\pi_3(S^2) \cong \mathbb{Z}$ — evaluated on the total space of the fibration, rather than just a product of two independently projected geometric volumes. This invariant equals the integer winding number counting how many times the S^1 fiber winds around the S^2 base under the standard Hopf map $S^3 \to S^2$. For the standard Hopf fibration this winding number is exactly 1.

The temporal branch projection $\Pi_{\text{time}} = \frac{1}{2}$ is a *continuous* rescaling acting on densities and trajectory-integrated geometric volumes. A continuous rescaling cannot change a topological winding number: applying Πtime to the cross term would yield a non-integer Hopf invariant, which is geometrically forbidden since $\pi_3(S^2) \sim= \mathbb{Z}$ admits no fractional elements. Therefore the cross term enters α^{-1} with coefficient exactly 1, as a direct consequence of the integrality of the Hopf invariant. The pure-volume terms $\frac{1}{2}\mathrm{Vol}(S^3)$ and $\frac{1}{2}\mathrm{Vol}(S^1)$ carry no such topological protection: they measure the sizes of spaces traversed by observable trajectories within the selected temporal branch, and trajectory-integrated quantities are legitimately halved by Πtime. The full expression for the leading geometric term is therefore

$$\alpha^{-1}_{\text{leading}} = \underbrace{\mathrm{Vol}(S^1)\cdot\mathrm{Vol}(S^3)}_{\text{Hopf term (topological, coeff. =1)}} + \underbrace{\tfrac{1}{2}\,\mathrm{Vol}(S^3) + \tfrac{1}{2}\,\mathrm{Vol}(S^1)}_{\text{branch-projected geometric volumes}} = 4\pi^3 + \pi^2 + \pi \qquad (3)$$

The distinction is thus between *topological integers,* which are invariant under Π_{time}, and *geometric volumes,* which are scalable by Π_{time}. This mirrors precisely the two-measure philosophy of HHQM at the cosmological level: the Haar measure encodes structural/topological information immune to metric rescaling, while the Lebesgue measure encodes geometric/metric content that scales with the FLRW volume form. The same dichotomy reappears here at the microscopic level inside the monocosm fibers $\mathbb{H}^\circ$, providing a unified conceptual thread across both the cosmological and the fine-structure-constant sectors of the framework.

Substituting exact volumes (Vol(S^1) = 2π, Vol(S^3) = $2\pi^2$) gives the leading geometric term

$$\alpha^{-1}_{\text{leading}} = 4\pi^3 + \pi^2 + \pi \approx 137.03630378.$$

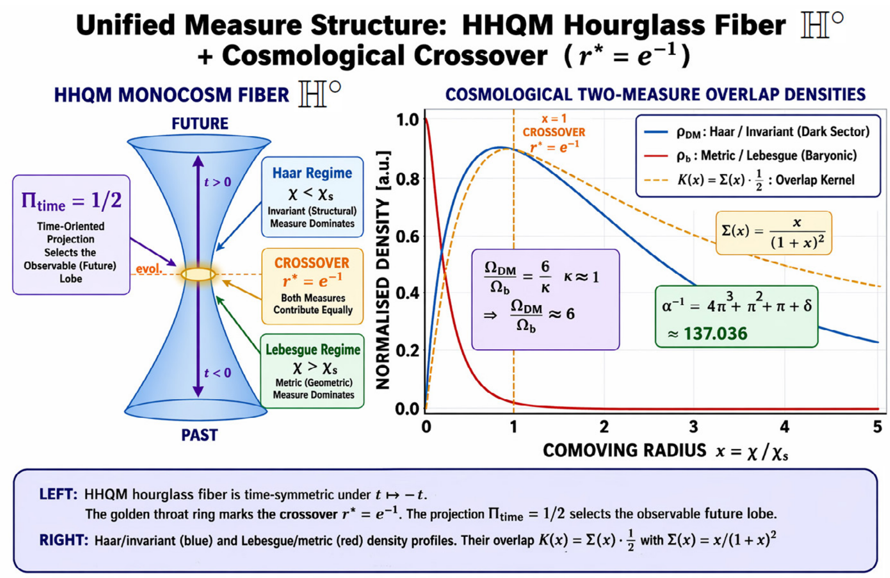

Figure 4: Unified geometric origin of dark-matter and α. HHQM hourglass fiber $\mathbb{H}^\circ$ (left, Π_{time} = 1/2) and cosmological densities (right). Single kernel $K = \Sigma(x)\Pi_{\text{time}}$ at $r^* = e^{-1}$ yields the selfterm weighting in α^{-1}.

The Hopf fibration structure connects directly to the matter-antimatter distinction via the topological charge sign in the $U(1)$ fiber. Due to absence of kinematic singularities in HHQM and, possibly, in HHQM-based field theories, the issue of the running value of α is not discussed here and remains an open problem.

The lead value (see also [49]) is still subject to higher order vista corrections derived from kernel curvature, and "soft" parameters like propensity distribution and crossover scale, which is an open problem. However, it is close enough to the current CODATA to justify further research. Future nuclear-clock and spectroscopic data (2025–2026) are predicted to shift the central value upward by ≈ +0.000305 as the vista term vanishes in the infinite-precision limit.

14. Conclusion and Predictions

Thus, we started exploring the intriguing possibility that dark matter, dark energy, and finestructure constant α are not independent mysteries but three manifestations of one geometric mechanism: the interplay of metric and invariant measures at the universal crossover $r^* = e^{-1}$. The framework seems to reproduces the observed abundance ratio, preserves ΛCDM background expansion, suppresses late-time growth, and predicts the value of α — with no free parameters. The transition from standard ΛCDM to this measure-theoretic description within the HHQM framework appears to be smooth, fully geometric, and directly falsifiable with existing instruments. If confirmed experimentally, it could offer a unified, parameter-free interpretation of several central open questions in contemporary physics.

Key testable signatures

- Suppressed $f\sigma_8(z)$ and reduced lensing amplitude at low redshift.
- Enhanced ISW effect.
- Upward refinement of α^{-1} toward 137.03630 in next-generation precision measurements.

Declarations

Consent to Publish. On behalf of both authors, the corresponding author declares that we consent to publish. Consent to Participate declaration: not applicable.

Funding Declaration: No / Not applicable.

Author Contribution: Both authors contributed equally, except for software development and application, where PT was the lead author.

Competing Interest Declaration: On behalf of both authors, the corresponding author declares that there is no competing interest.

Ethics declaration: not applicable.

References

1. Abbott, T. M., Aguena, M., Alarcon, A., Allam, S., Alves, O., Amon, A., ... & Smith, M. (2022). Dark Energy Survey Year 3 results: Cosmological constraints from galaxy clustering and weak lensing. Physical Review D, 105(2), 023520.
2. Adler, S. L. (1995). *Quaternionic Quantum Mechanics and Quantum Fields,* Oxford University Press, Oxford, UK.
3. Aghanim, N. (2020). Planck 2018 results. VI. Cosmological parameters. Astron. Astrophys, 641, A6.
4. Asgari, M., Lin, C. A., Joachimi, B., Giblin, B., Heymans, C., Hildebrandt, H., ... & Valentijn, E. (2021). KiDS-1000 cosmology: Cosmic shear constraints and comparison between two point statistics. Astronomy & Astrophysics, 645, A104.
5. Ashtekar, A., & Schilling, T. A. (1999). Geometrical formulation of quantum mechanics. In On Einstein's Path: essays in honor of Engelbert Schucking (pp. 23-65). New York, NY: Springer New York.
6. Bengtsson, I., & Życzkowski, K. (2017). Geometry of quantum states: an introduction to quantum entanglement. Cambridge university press.
7. Blumenthal, G. R., Faber, S. M., Primack, J. R., & Rees, M. J. (1984). Formation of galaxies and large-scale structure with cold dark matter. Nature, 311(5986), 517-525.
8. Brody, D. C., Hughston, L. P. (2001). "Geometric quantum mechanics." Journal of Geometry and Physics, 38(1), 19-53.
9. Pantos, I., & Perivolaropoulos, L. (2026). Status of the S8 tension: A 2026 review of probe discrepancies. Physics of the Dark Universe, 102286.
10. Cirelli, R., Manià, A., & Pizzocchero, L. (1990). Quantum mechanics as an infinite-dimensional Hamiltonian system with uncertainty structure: Part II. Journal of Mathematical Physics, 31(12), 2898-2903.
11. Crittenden, R. G., & Turok, N. (1996). Looking for a cosmological constant with the Rees-Sciama effect. Physical Review Letters, 76(4), 575.
12. Schmidt, F. (2008). Weak lensing probes of modified gravity. Physical Review D—Particles, Fields, Gravitation, and Cosmology, 78(4), 043002.
13. Adame, A. G., Aguilar, J., Ahlen, S., Alam, S., Alexander, D. M., Alvarez, M., ... & Rich, J. (2025). DESI 2024 VI: cosmological constraints from the measurements of baryon acoustic oscillations. Journal of Cosmology and Astroparticle Physics, 2025(02), 021.
14. DESI Collaboration, Abdul Karim, M., Adame, A. G., Aguado, D., Aguilar, J., Ahlen, S., ... & Krolewski, A. (2026). Data release 1 of the dark energy spectroscopic instrument. The Astronomical Journal, 171(5), 285.
15. Donaldson, S. K. (2001). Scalar curvature and projective embeddings, I. Journal of Differential Geometry, 59(3), 479-522.
16. Einasto, J. (1965). On the Construction of a Composite Model for the Galaxy and on the Determination of the System of Galactic Parameters. Trudy Astrofizicheskogo Instituta Alma-Ata, Vol. 5, p. 87-100, 1965, 5, 87-100.
17. Gaeta, G., & Morando, P. (2002). Hyper-Hamiltonian dynamics. Journal of Physics A: Mathematical and General, 35(17), 3925-3943.

18. Giachetta, G., Mangiarotti, L., & Sardanashvily, G. A. (2010). Geometric formulation of classical and quantum mechanics. World Scientific.
19. Guendelman, E. I., & Kaganovich, A. B. (1996). Principle of nongravitating vacuum energy and some of its consequences. Physical Review D, 53(12), 7020.
20. Guendelman, E., Nissimov, E., & Pacheva, S. (2015). Dark energy and dark matter from hidden symmetry of gravity model with a non-Riemannian volume form. The European Physical Journal C, 75(10), 472.
21. Guendelman, E., Nissimov, E., & Pacheva, S. (2015, June). Metric-independent spacetime volume-forms and dark energy/dark matter unification. In International Workshop on Lie Theory and Its Applications in Physics (pp. 261-273). Singapore: Springer Singapore.
22. Guendelman, E., Nissimov, E., & Pacheva, S. (2015, June). Metric-independent spacetime volume-forms and dark energy/dark matter unification. In International Workshop on Lie Theory and Its Applications in Physics (pp. 261-273). Singapore: Springer Singapore.
23. Guendelman, E., & Herrera, R. (2024). Unification: Emergent universe followed by inflation and dark epochs from multi-field theory. Annals of Physics, 460, 169566.
24. Guendelman, E., & Herrera, R. (2025). Unifying inflation, dark energy, and dark matter with a scalar field and exotic fermions. Physical Review D, 112(2), 023542.
25. Haar, A. (1933). Der Massbegriff in der Theorie der kontinuierlichen Gruppen. Annals of mathematics, 34(1), 147-169.
26. Halmos, P. R. (1974). Measure Theory Springer. New York.
27. Heydari, H. (2015). Geometric formulation of quantum mechanics. arXiv preprint arXiv:1503.00238.
28. Hitchin, N. J. (1990). "Flat connections and geometric quantization." Communications in Mathematical Physics, 131(2), 347-380.
29. Kibble, T. W. (1979). Geometrization of quantum mechanics. Communications in Mathematical Physics, 65(2), 189-201.
30. Kostant, B. (1973). Quantization and unitary representations. Uspekhi Matematicheskikh Nauk, 28(1), 163-225.
31. Leibniz, G. W. (1991). Discourse on metaphysics and other essays. Hackett Publishing.
32. Lin, M. X., Jain, B., Raveri, M., Baxter, E. J., Chang, C., Gatti, M., ... & Muir, J. (2024). Late time modification of structure growth and the S 8 tension. Physical Review D, 109(6), 063523.
33. Linder, E. V. (2005). Cosmic growth history and expansion history. Physical Review D—Particles, Fields, Gravitation, and Cosmology, 72(4), 043529.
34. Nakahara, M. (2018). Geometry, topology and physics. CRC press.
35. Navarro, J. F. (1996, January). The structure of cold dark matter halos. In Symposium-international astronomical union (Vol. 171, pp. 255-258). Cambridge University Press.
36. Kazantzidis, L., & Perivolaropoulos, L. (2018). Evolution of the f σ 8 tension with the Planck 15/Λ CDM determination and implications for modified gravity theories. Physical Review D, 97(10), 103503.
37. Nguyen, N. M., Huterer, D., & Wen, Y. (2023). Evidence for suppression of structure growth in the concordance cosmological model. Physical Review Letters, 131(11), 111001.
38. Peebles, P. J. E. (2020). The large-scale structure of the universe.
39. Peter, P., Uzan, J.-P., Cosmology (Oxford University Press, 2013).
40. Primack, J. R. (1997). Dark matter and structure formation in the Universe. arXiv preprint astro-ph/9707285.
41. Terasawa, R., Takada, M., Kurita, T., & Sugiyama, S. (2025). Late-time suppression of structure growth as a solution for the S 8 tension. Physical Review D, 112(8), 083556.
42. Trifonov, V. (1995). A linear solution of the four-dimensionality problem. EPL (Europhysics Letters), 32(8), 621-626.
43. Trifonov, V. (2007). Natural geometry of nonzero quaternions. International Journal of Theoretical Physics, 46(2), 251-257.
44. Trifonov, V. (2008). GR-friendly description of quantum systems. International Journal of Theoretical Physics, 47(2), 492-510.
45. Trifonov, V. (2011). Geometric Modification of Quantum Mechanics, in "Focus on Quantum Mechanics", Editors David E. Hathaway et al., Nova Publishers, Physics Research and Technology, N.Y. pp. 15-34.
46. Trifonov, V. Geometric Amplitude Formulation of Measurement in Hyperhamiltonian Quantum Mechanics. Available at SSRN 6732470.
47. Weinberg, S., (1972). Gravitation and Cosmology (Wiley, 1972).
48. Woodhouse, N. M. J. (1992). Geometric quantization. Oxford university press.
49. Wyler, A., (1971). Phys. Today 24 (8) 17.